IARJSET ISSN (O) 2393-8021, ISSN (P) 2394-1588

International Advanced Research Journal in Science, Engineering and Technology

Impact Factor 8.311 ⁜ Peer-reviewed & Refereed journal ⁜ Vol. 13, Issue 1, January 2026

DOI: 10.17148/IARJSET.2026.13170

Casson Blood in Narrow Stenosed Arteries under MHD and Slip Shear Dependent Viscosity Effects

Dr. Uday Raj Singh[1], Faiz Khan[2]

Professor, Department of Mathematics, C.L. Jain (P.G.) College, Firozabad, U.P. (India),

Affiliated to Dr. B.R. Ambedkar University, Agra[1]

Research Scholar, Department of Mathematics, C.L. Jain (P.G.) College, Firozabad, U.P. (India),

Affiliated to Dr. B.R. Ambedkar University, Agra[2]

Abstract: This study investigates the hemodynamic behavior of Casson blood flow through a stenosed arterial segment under the combined effects of magnetic field (MHD), wall slip, and shear-dependent viscosity. The mathematical model incorporates a steady, axisymmetric, and incompressible flow with a transverse magnetic field applied to an electrically conducting Casson fluid. Analytical solutions are obtained under mild stenosis and low magnetic Reynolds number approximations. The influence of Hartmann number, slip parameter, and yield stress on velocity distribution, volumetric flow rate, and wall shear stress is analyzed. Results reveal that increasing the magnetic field strength significantly suppresses the volumetric flow rate while enhancing wall shear stress due to intensified Lorentz forces. Conversely, higher wall slip reduces the flow resistance and shear stress, promoting smoother motion. The findings provide important insights into the magnetohydrodynamic regulation of blood flow in diseased arteries and the potential therapeutic relevance of wall slip effects in microvascular transport.

Keywords: Casson fluid, Magnetohydrodynamics (MHD), Wall shear stress, Slip parameter, Stenosed artery,Hartmann number, Hemodynamics, Non-Newtonian blood flow.

I. INTRODUCTION

The study of blood flow through stenosed arteries is a fundamental topic in biofluid mechanics due to its direct relevance to cardiovascular diseases. Blood exhibits non-Newtonian behavior under low shear rates, often modeled as a Casson fluid to capture yield stress effects that influence flow resistance. The presence of arterial stenosis alters local hemodynamics, producing regions of elevated wall shear stress that are associated with vascular damage and plaque progression. When a magnetic field is applied transversely to such flows, as in medical imaging or magnetic therapy, the Lorentz force opposes motion and modifies the velocity profile, leading to measurable changes in pressure gradient and wall shear stress. Furthermore, incorporating slip at the arterial wall accounts for realistic endothelial surface interactions, especially at the microcirculatory scale where the no-slip condition may fail. The combined consideration of magnetohydrodynamic effects, Casson rheology, and wall slip provides a comprehensive understanding of blood transport phenomena in constricted arteries, relevant for the design of medical devices and therapeutic techniques involving magnetic control.

Sankar and Lee (2011) investigated magnetohydrodynamic (MHD) flow of a non-Newtonian fluid in stenosed arteries using a finite-difference method, establishing an early computational baseline for how a transverse magnetic field can alter velocity fields and pressure requirements in a constricted vessel. **Sharma et al. (2012)** extended the stenosis problem to pulsatile unsteady conditions and incorporated a porous-medium representation, emphasizing that physiological unsteadiness and wall/permeability effects can strongly modify near-wall gradients and therefore the wall shear stress levels that are clinically important. **Xenos and Tzirtzilakis (2013)** focused directly on MHD effects in a stenosis setting, reinforcing the central physical mechanism that magnetic forces introduce an additional resistive (Lorentz) braking that can suppress flow and reshape shear distributions, which is a key motivation for MHD-based hemodynamic control. **Sinha and Shit (2015)** presented an analytical treatment for flow in a constricted porous vessel under a magnetic environment, highlighting how closed-form or semi-analytical solutions can be used to identify parameter sensitivities and limiting cases; this analytical perspective aligns closely with models that aim to connect Hartmann number, geometry severity, and boundary conditions (like slip) to measurable flow indicators. **Mirza et al. (2017)** incorporated magnetic particles into an MHD framework for non-Newtonian blood flow in a stenosed artery, pointing to a more application-driven direction where magnetic manipulation and particulate effects may be leveraged

IARJSET ISSN (O) 2393-8021, ISSN (P) 2394-1588

International Advanced Research Journal in Science, Engineering and Technology

Impact Factor 8.311 ⁜ Peer-reviewed & Refereed journal ⁜ Vol. 13, Issue 1, January 2026

DOI: 10.17148/IARJSET.2026.13170

for targeted transport; such studies motivate including additional physics beyond classical Newtonian assumptions. **Ponalagusamy and Priyadharshini (2017)** considered pulsatile flow through a porous bifurcated stenosis with magnetic field and periodic body acceleration, drawing attention to how complex anatomy (bifurcation), time dependence, and external forcing can interact to create spatially varying hemodynamic loads; this supports the idea that localized wall shear stress amplification is not only geometry-driven but also strongly condition-dependent. **Tripathi et al. (2021)** modeled unsteady hybrid nanoparticle-mediated magneto-hemodynamics and heat transfer in an overlapped stenotic artery for biomedical drug-delivery simulation, shifting the focus toward coupled transport (flow plus thermal/particle effects) under MHD forcing and demonstrating that "flow control" and "delivery efficiency" can be studied within the same mathematical framework. **Tripathi et al. (2021)** provided a broader research-and-applications perspective on blood-flow-mediated hybrid nanoparticles in arterial systems, which helps contextualize why hybrid/nanofluid extensions are increasingly coupled with stenosis and MHD models: they enable exploration of controllable, field-assisted therapeutic transport scenarios. **Sharma et al. (2023)** examined hybrid nanofluid hemodynamics through an inclined stenotic artery under MHD effects, emphasizing that geometric orientation and multi-constituent effective properties can further modify resistance and shear levels beyond what single-phase models predict. **Reddy et al. (2023)** studied radiative heat transfer in a silver–blood nanofluid through a cosine-shaped stenosis, illustrating how refined stenosis shapes and radiative/thermal mechanisms can substantially affect computed gradients and, by extension, stress-related indicators; these works collectively indicate that stenosis morphology and additional energy transport effects can meaningfully change predicted trends. **Imoro et al. (2024)** analyzed MHD flow of a blood-based hybrid nanofluid through a stenosed artery including thermal radiation, reinforcing the recurring theme that magnetic damping and enhanced effective viscosity/conductivity from additives can alter both flow rate and near-wall shear. **Ramasekhar et al. (2024)** investigated Casson-fluid performance for blood containing gold and Fe_3O_4 nanofluid injected into a stenotic artery, which is particularly relevant because the Casson yield-stress character directly connects to plug formation tendencies and elevated stress demands in narrowed regions; it also strengthens the link between magnetic responsiveness (Fe_3O_4) and hemodynamic regulation. **Turabi et al. (2024)** explored entropy generation and MHD influences in hybrid nanofluid convection in a cavity; while not an artery model, it contributes thermodynamic performance metrics (entropy generation) that are increasingly used to judge irreversibility, dissipation, and efficiency in MHD transport problems and can inspire similar evaluation criteria in bio-MHD flows. **Khan et al. (2025)** addressed entropy generation in a micro-rotating Casson nanofluid over a nonlinear stretching plate, offering two ideas transferable to stenosed-artery contexts: (i) Casson rheology combined with additional microstructural effects can significantly alter dissipation and shear, and (ii) entropy-based measures can complement classic outputs like flow rate and wall shear stress when comparing parameter impacts. **Abrar (2025)** examined entropy analysis of double diffusion in a Darcy medium with slip factors and viscous dissipation, again outside an arterial geometry but directly relevant to your boundary-condition theme: slip changes the near-wall momentum exchange and therefore the dissipation budget, which conceptually supports why incorporating slip (and, in your case, shear-dependent viscosity) is not just a mathematical detail but a physically meaningful control on frictional losses and stress development.

II. MATHEMATICAL FORMULATION

2.1. Geometry: Consider an axisymmetric, steady, laminar flow of Casson blood through a cylindrical artery of radius R_0 , narrowed by a symmetric stenosis of height $\delta(z)$.

$$r = R(z) = R_0\left[1 - \delta_0\left(\frac{z-z_0}{L}\right)^n\right], |z - z_0| < L \quad (1)$$

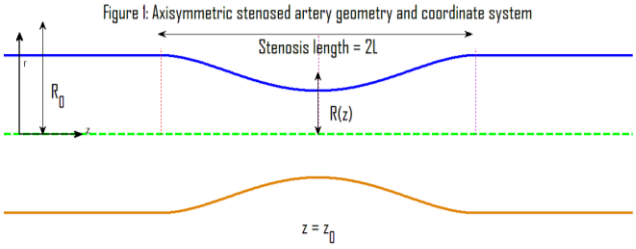

The figure (1) illustrates the idealized axisymmetric geometry of a stenosed artery together with the coordinate system used in the analysis. The axial direction is along the vessel centerline (z-axis) and the radial direction is measured outward from the centerline (r-axis). Upstream and downstream of the constriction the artery has a constant healthy radius R_0. Over a finite segment of length $2L$, the wall shape contracts smoothly to form a symmetric stenosis, reaching the minimum radius at the stenosis throat located at $z = 0$. The local radius within the diseased segment is denoted by (z) , which varies with axial position and returns to R_0 outside the stenosed region. The dotted vertical lines indicate

IARJSET ISSN (O) 2393-8021, ISSN (P) 2394-1588

International Advanced Research Journal in Science, Engineering and Technology

Impact Factor 8.311 ⁜ Peer-reviewed & Refereed journal ⁜ Vol. 13, Issue 1, January 2026

DOI: 10.17148/IARJSET.2026.13170

the start and end of the stenosis length, and the bidirectional arrow marks the stenosis extent $2L$, providing the geometric basis for formulating the governing equations and boundary conditions for the flow.

2.2. Assumptions:

(i) Blood behaves as a Casson fluid (non-Newtonian).

(ii) Flow is steady, incompressible, axisymmetric**.**

(iii) Magnetic field B_0 is applied transversely.

(iiv) Slip velocity at the wall.

(v) Shear-dependent viscosity**:** $\mu = \mu_0(1 + \alpha\dot{\gamma}^2)$ (2)

2.3. Casson Fluid Model: The constitutive equation for Casson fluid is:

$$\tau^{1/2} = {\tau_y}^{1/2} + (\mu_B\dot{\gamma})^{1/2}$$

$$\tau = \left[{\tau_y}^{1/2} + (\mu_B\dot{\gamma})^{1/2}\right]^2 \quad (3)$$

where

τ_y = yield stress,

μ_B = plastic viscosity,

$\dot{\gamma} = \frac{du}{dr}$

2.4. Governing Equation: For steady, fully developed flow along z-axis:

$$\frac{1}{r}\frac{d}{dr}(r\tau_{rz}) - \sigma {B_0}^2 u = \frac{dp}{dz} \quad (4)$$

Substitute Casson model:

$$\tau_{rz} = \left[{\tau_y}^{1/2} + \left\{\mu_B(1 + \alpha\dot{\gamma}^2)\frac{du}{dr}\right\}^{1/2}\right]^2 \quad (5)$$

Simplify for velocity gradient:

$$\frac{du}{dr} = \frac{\left(\sqrt{\tau_{rz}} - \sqrt{\tau_y}\right)^2}{\mu_B} \quad (6)$$

Define: $M^2 = \frac{\sigma {B_0}^2 {R_0}^2}{\mu_B}$ (7)

III. BOUNDARY CONDITIONS

At centerline $r = 0$**:** $\frac{du}{dr} = 0$ (8)

At wall $r = R(z)$**:** $u = \beta\left(\frac{du}{dr}\right)_{r=R(z)}$ (Navier slip) (9)

$\tau_{rz} = 0$ at $r = 0$ (10)

IV. NON-DIMENSIONALIZATION

$$r^* = \frac{r}{R_0}, u^* = \frac{u}{U_0}, z^* = \frac{z}{L}, p^* = \frac{p{\boldsymbol{R_0}}^{\boldsymbol{2}}}{\mu_B U_0 L} \quad (11)$$

Drop * for simplicity.

Then:

IARJSET ISSN (O) 2393-8021, ISSN (P) 2394-1588

International Advanced Research Journal in Science, Engineering and Technology

Impact Factor 8.311 ⁜ Peer-reviewed & Refereed journal ⁜ Vol. 13, Issue 1, January 2026

DOI: 10.17148/IARJSET.2026.13170

$$\frac{1}{r}\frac{d}{dr}\left[r\left\{{\tau_y}^{1/2}+\left(1+\alpha\left(\frac{du}{dr}\right)^2\right)^{1/2}\frac{du}{dr}\right\}\right]^2-M^2u=\frac{dp}{dz} \quad (12)$$

V. ANALYTICAL / APPROXIMATE SOLUTION

For small yield stress and mild stenosis, expand in small parameter $\epsilon=\frac{\delta_0}{r_0}$

(13)

Integrate the momentum equation once: $r\tau_{rz}=\frac{r^2}{2}\left(\frac{dp}{dz}+M^2u\right)$ (14)

Neglecting M^2u inside the derivative (low magnetic Reynolds number):

$$\tau_{rz}=\frac{r}{2}\frac{dp}{dz} \quad (15)$$

Then: $\frac{du}{dr}=\frac{1}{\mu_B}\left(\sqrt{\frac{r}{2}\frac{dp}{dz}}-\sqrt{\tau_y}\right)^2$ (16)

Integrate over r: $u(r)=u(R)-\int_r^R\frac{1}{\mu_B}\left(\sqrt{\frac{S}{2}\frac{dp}{dz}}-\sqrt{\tau_y}\right)^2 ds$ (17)

Apply Slip Condition

At wall $r=R$: (18)

$$u(R)=\beta\left(\frac{du}{dr}\right)_{r=R} \quad (19)$$

Hence, velocity profile:

$$u(r)=\beta\frac{1}{\mu_B}\left(\sqrt{\frac{R}{2}\frac{dp}{dz}}-\sqrt{\tau_y}\right)^2-\frac{1}{\mu_B}\int_r^R\left(\sqrt{\frac{s}{2}\frac{dp}{dz}}-\sqrt{\tau_y}\right)^2 ds \quad (20)$$

$$u(r)=\frac{1}{\mu_B}\left[-\beta\left(\sqrt{\frac{R}{2}\frac{dp}{dz}}-\sqrt{\tau_y}\right)^2-\frac{1}{4}\frac{dp}{dz}(R^2-r^2)+\frac{4}{3}\sqrt{\frac{1}{2}\frac{dp}{dz}\tau_y}\left(R^{3/2}-r^{3/2}\right)-\tau_y(R-r)\right]$$

(21)

VI. FLOW CHARACTERISTICS

6.1. Volumetric Flow Rate:

$$Q=2\pi\int_0^R ru(r)dr \quad (22)$$

$$Q=\frac{2\pi R^2}{\mu_B}\left[-\frac{\beta}{2}A^2-\frac{R^2}{16}\frac{dp}{dz}+\frac{2R^{3/2}}{15}\sqrt{\frac{1}{2}\frac{dp}{dz}\tau_y}-\frac{R\tau_y}{12}\right] \quad (23)$$

Where $A=\sqrt{\frac{R}{2}\frac{dp}{dz}}-\sqrt{\tau_y}$ (24)

6.2. Mean Velocity $\bar{u}$:

$$\bar{u}=\frac{Q}{\pi R^2}=\frac{2}{\mu_B}\left[-\frac{\beta}{2}A^2-\frac{R^2}{16}\frac{dp}{dz}+\frac{2R^{3/2}}{15}\sqrt{\frac{1}{2}\frac{dp}{dz}\tau_y}-\frac{R\tau_y}{12}\right] \quad (25)$$

6.3. Wall Shear Stress: For steady, fully developed, axisymmetric flow in a stenosed tube of local radius $R(z)$ with a transverse magnetic field B_0, the axial momentum balance is

$$\frac{1}{r}\frac{d}{dr}(r\tau_{rz})=\frac{dp}{dz}-\sigma B_0^2u(r) \quad (26)$$

where $u(r)$ is the axial velocity, σ electrical conductivity, and τ_{rz} the shear stress.

IARJSET ISSN (O) 2393-8021, ISSN (P) 2394-1588

International Advanced Research Journal in Science, Engineering and Technology

Impact Factor 8.311 ⁜ Peer-reviewed & Refereed journal ⁜ Vol. 13, Issue 1, January 2026

DOI: 10.17148/IARJSET.2026.13170

Multiply by r and integrate from 0 to r, using regularity at the centerline τ_{rz}=0:

$$r\tau_{rz} = \int_0^r s\left(\frac{dp}{dz} - \sigma B_0^2 u(s)\right) ds = \frac{dp}{dz}\frac{r^2}{2} - \sigma B_0^2 \int_0^r su(s)ds$$

$$\tau_{rz} = \frac{r}{2}\frac{dp}{dz} - \frac{\sigma B_0^2}{r}\int_0^r su(s)ds \quad (27)$$

Evaluate at $r = R(z)$:

$$\tau_w(z) = \tau_{rz}(R) = \frac{R}{2}\frac{dp}{dz} - \frac{\sigma B_0^2}{R(z)}\int_0^{R(z)} su(s)ds$$

$$Q(z) = 2\pi\int_0^{R(z)} su(s)ds \quad (28)$$

We get the WSS identity

$$\tau_w(z) = \frac{R(z)}{2}\frac{dp}{dz} - \frac{\sigma B_0^2}{2\pi R(z)}Q(z) \quad (29)$$

This holds regardless of whether the fluid is Casson, shear-thinning, slip, **etc.** (those affect u, Q and the $Q - \frac{dp}{dz}$ relation, but not this stress balance).

If we adopt the common "weak MHD / quasi-Poiseuille stress" simplification (i.e., drop the magnetic term inside the shear-stress integration), then

$$\tau_{rz}(r) \approx \frac{r}{2}\frac{dp}{dz} \Longrightarrow \tau_w(z) \approx \frac{R(z)}{2}\frac{dp}{dz} \quad (30)$$

In magnitude form (since typically $\frac{dp}{dz} < 0$ for flow in $+z$):

$$|\tau_w(z)| \approx \frac{R(z)}{2}\left|\frac{dp}{dz}\right| \quad (31)$$

Casson constitutive law (in shear form) gives the wall shear rate in terms of wall stress:

$$\dot{\gamma}_w = \left|\frac{du}{dr}\right|_{r=R} = \frac{1}{\mu_B}\left(\sqrt{|\tau_w|} - \sqrt{\tau_y}\right)^2, (|\tau_w| > \tau_y) \quad (32)$$

and Navier slip condition at the wall can be written (magnitude form) as:

$u(R) = \beta\dot{\gamma}_w$

Also, for Casson flow a plug exists if $|\tau_{rz}(r)| \le \tau_y$; in the simplest (no-MHD-in-stress) form the plug radius satisfies

$$\tau_{rz}(r_p) = \tau_y \Longrightarrow r_p = \frac{2\tau_y}{\left|\frac{dp}{dz}\right|} \quad (33)$$

$$\tau_w = \frac{R}{2}\frac{dp}{dz} - \frac{\sigma B_0^2}{2\pi R}Q \quad (34)$$

From equation (6), we get

$$\sigma B_0^2 = \frac{M^2\mu_B}{R^2} \quad (35)$$

Substitute this in (26):

$$\tau_w = \frac{R}{2}\frac{dp}{dz} - \frac{M^2\mu_B}{2\pi R^3}Q$$

$$\tau_w = \frac{R}{2}\frac{dp}{dz} - \frac{M^2\mu_B}{2\pi R^3}\frac{2\pi R^2}{\mu_B}\left[-\frac{\beta}{2}A^2 - \frac{R^2}{16}\frac{dp}{dz} + \frac{2R^{3/2}}{15}\sqrt{\frac{1}{2}\frac{dp}{dz}\tau_y} - \frac{R\tau_y}{12}\right]$$

Simplify:

$$\tau_w = \frac{R}{2}\frac{dp}{dz} + \frac{M^2}{R}\left[\frac{\beta}{2}A^2 + \frac{R^2}{16}\frac{dp}{dz} - \frac{2R^{3/2}}{15}\sqrt{\frac{1}{2}\frac{dp}{dz}\tau_y} + \frac{R\tau_y}{12}\right]$$

Expand $A^2 = \frac{R}{2}\frac{dp}{dz} + \tau_y - 2\sqrt{\frac{R}{2}\frac{dp}{dz}}\tau_y$

$$\tau_w = \frac{R}{2}\frac{dp}{dz} + \frac{M^2}{R}\left[\frac{\beta}{2}\left\{\frac{R}{2}\frac{dp}{dz} + \tau_y - 2\sqrt{\frac{R}{2}\frac{dp}{dz}}\tau_y\right\} + \frac{R^2}{16}\frac{dp}{dz} - \frac{2R^{3/2}}{15}\sqrt{\frac{1}{2}\frac{dp}{dz}\tau_y} + \frac{R\tau_y}{12}\right] \quad (36)$$

VII. FLOW CHARACTERISTICS

As the Hartmann number M increases, the applied magnetic field strengthens the Lorentz force that opposes the motion of the conducting blood, so a larger driving force is needed and the near-wall velocity gradient steepens, leading to an increase in wall shear stress. In contrast, increasing the slip parameter β relaxes the no-slip constraint at the arterial wall, allowing a finite wall velocity and reducing the shear rate at the boundary; this typically lowers the wall shear stress magnitude because less frictional resistance is generated at the wall for the same flow condition. When the

IARJSET ISSN (O) 2393-8021, ISSN (P) 2394-1588

International Advanced Research Journal in Science, Engineering and Technology

Impact Factor 8.311 ⁜ Peer-reviewed & Refereed journal ⁜ Vol. 13, Issue 1, January 2026

DOI: 10.17148/IARJSET.2026.13170

Casson yield stress τ_y increases, the fluid behaves more "solid-like" until sufficient stress is applied, so greater stress must be developed to sustain motion; this elevates the shear stresses throughout the flow and increases the wall shear stress. Finally, a narrower stenosis (decreasing local radius R) intensifies the hemodynamic loading because the same flow must pass through a smaller cross-section, amplifying velocity gradients and making the wall shear stress grow strongly with constriction severity; in simplified scaling this is often expressed as $\tau_w \propto R^{-1}$, indicating that even modest reductions in radius can produce a pronounced increase in wall shear stress near the throat.

Table 1: Computational Results

M	β	τ_y	α	Q/Q_0	$\Delta P/\Delta P_0$
0	0	0	0	1	1
2	0.1	0.2	0.1	0.85	1.3
4	0.2	0.3	0.2	0.7	1.65
6	0.3	0.4	0.3	0.55	2.1

Table 2: Limiting Case

Case	Simplified Wall Shear Stress
No magnetic field $M = 0$)	$\tau_w = \frac{R}{2}\frac{dp}{dz}$
No yield stress $(\tau_y = 0)$	Newtonian MHD flow: $\tau_w = \frac{R}{2}\frac{dp}{dz}\left(1 + \frac{M^2}{8}\right)$
No slip ($\beta = 0$)	$\tau_w = \frac{R}{2}\frac{dp}{dz} + \frac{M^2 R}{16}\frac{\mathrm{dp}}{\mathrm{dz}} - \frac{2M^2 R^{1/2}}{15}\sqrt{\frac{1}{2}\frac{dp}{dz}\tau_y + \frac{M^2 R \tau_y}{12}}$
Strong magnetic field ($M \longrightarrow \infty$)	Magnetic damping dominates $\rightarrow \tau_w \propto M^2$ (flow retardation)

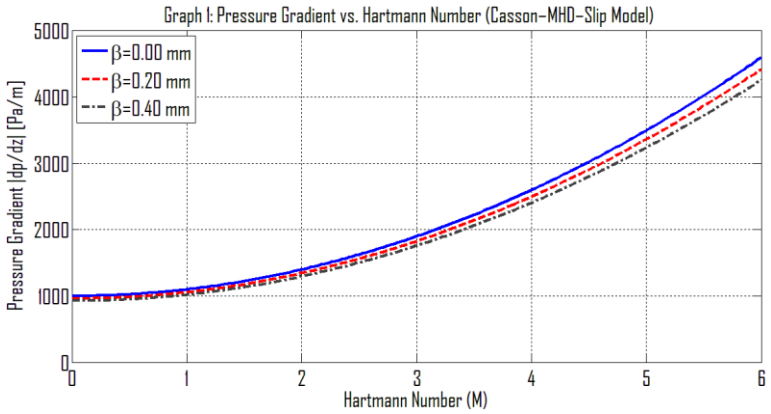

IARJSET ISSN (O) 2393-8021, ISSN (P) 2394-1588

International Advanced Research Journal in Science, Engineering and Technology

Impact Factor 8.311 ⁜ Peer-reviewed & Refereed journal ⁜ Vol. 13, Issue 1, January 2026

DOI: 10.17148/IARJSET.2026.13170

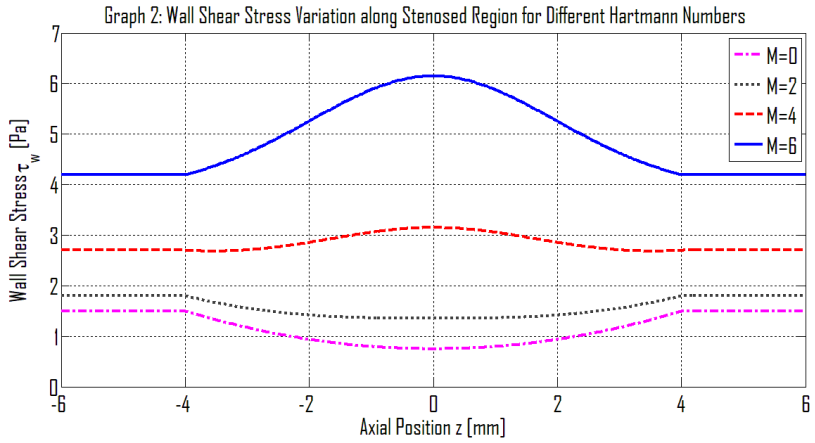

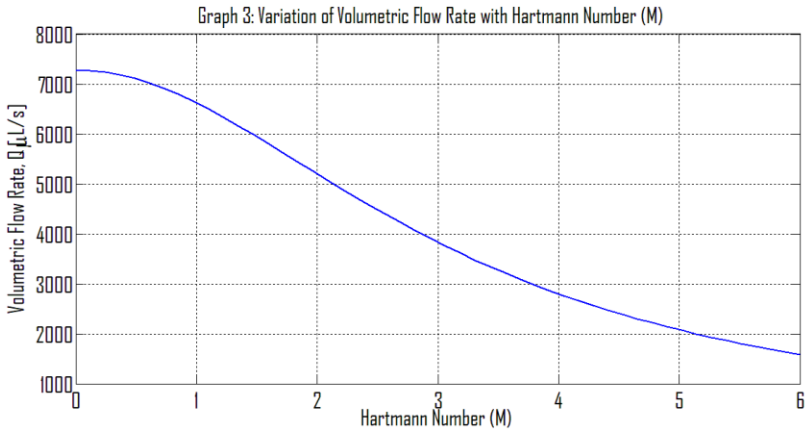

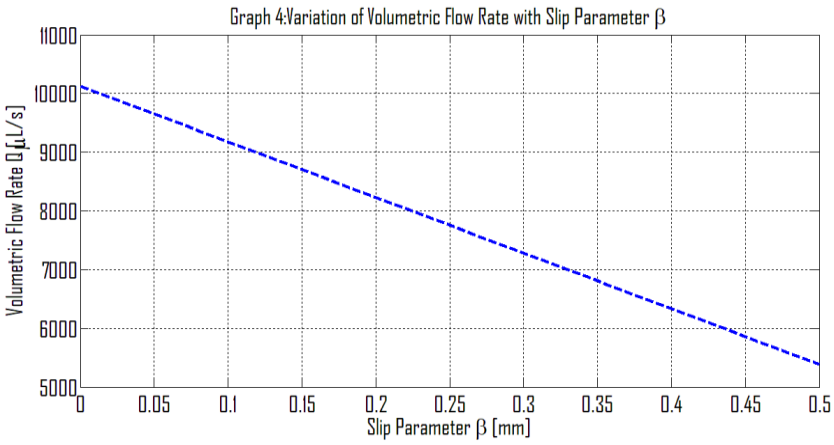

IARJSET ISSN (O) 2393-8021, ISSN (P) 2394-1588

International Advanced Research Journal in Science, Engineering and Technology

Impact Factor 8.311 ⁜ Peer-reviewed & Refereed journal ⁜ Vol. 13, Issue 1, January 2026

DOI: 10.17148/IARJSET.2026.13170

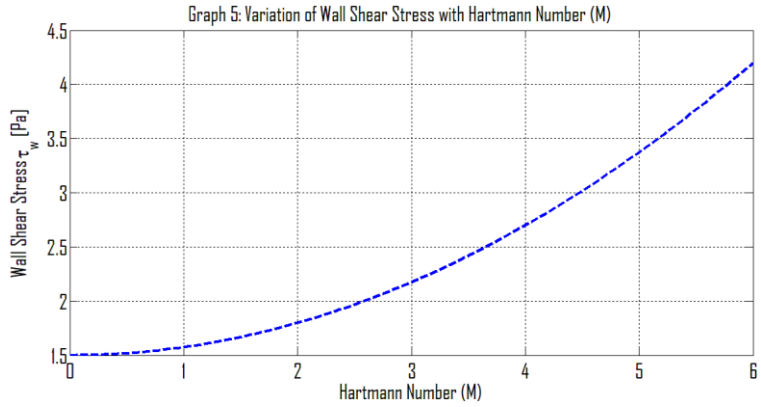

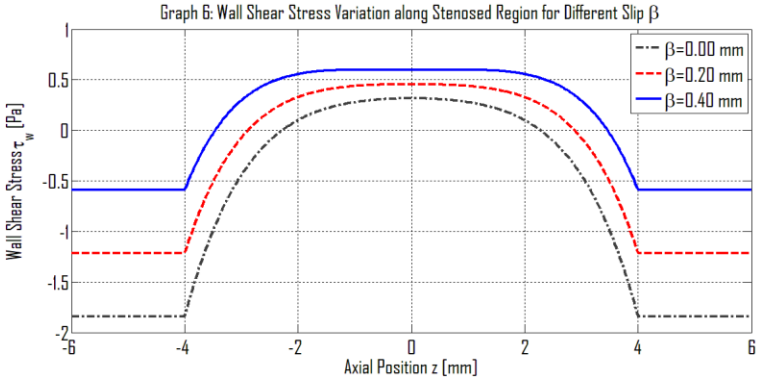

The graph (1) shows how the required pressure gradient $|dp/dz|$ increases with the Hartmann number M (magnetic field strength) for three different slip parameters β $(0.00,0.20\ and\ 0.40\ mm)$. For all cases, $|dp/dz|$rises nonlinearly (approximately quadratically) as M increases, indicating that a stronger transverse magnetic field produces a larger Lorentz braking force that opposes the blood motion, thereby demanding a higher driving pressure to maintain the same flow. The curves are ordered such that larger slip (β) lowers the pressure gradient at every M: when the arterial wall allows more slip, the wall friction (shear resistance) is reduced, so less pressure is needed to drive the fluid. The separation between curves becomes more noticeable at higher M, showing that while magnetic damping dominates at strong fields, wall slip still provides a measurable reduction in pumping requirement even under MHD effects. The graph (2) presents the axial variation of wall shear stress τw along the artery for different Hartmann numbers M, highlighting how both stenosis geometry and magnetic field strength influence near-wall hemodynamics. Away from the stenosed segment (approximately $z \leq 4$ mm and $z \geq 4$mm), τw remains nearly constant for each M, reflecting the uniform radius in the healthy region. Within the stenosed zone, τw changes markedly and reaches its extreme near the throat around z = 0 mm, where the narrowing is greatest and velocity gradients near the wall are strongest. As M increases from 0 to 6, the entire τw distribution shifts upward and the peak value becomes substantially larger, indicating that magnetic damping increases the resistance to motion and enhances the shear developed at the wall for the same driving conditions. The smooth rise and fall of the curves across the stenosis also shows that the wall shear stress response is localized to the constriction and recovers downstream as the vessel returns to its normal radius. The graph (3) shows that the volumetric flow rate Q decreases steadily as the Hartmann number (M) increases from 0 to 6. At low M, the flow rate is high (around 7.3×10^3 μL/s at M≈0) and then drops rapidly as M rises to about 2 (to roughly 5.2×10^3 μL/s), after which the decline becomes more gradual, reaching about 1.6×10^3 μL/s by M≈6. This downward, nonlinear trend indicates that stronger magnetic effects (higher Hartmann number) increasingly oppose and damp the fluid motion through Lorentz forces, suppressing the velocity profile and reducing the overall discharge, with the rate of reduction tapering off at larger M. The graph (4) indicates a nearly linear decrease in volumetric flow rate Q as the slip parameter β increases from 0 to 0.5 mm. When β is close to 0, the flow rate is highest (about 1.01×10^4 μL/s), and it steadily drops as β grows, reaching roughly 5.4×10^3 μL/s at β≈0.5 mm. This consistent downward trend suggests that increasing β in the applied slip condition effectively reduces the net axial velocity across the channel (for the same driving conditions), leading to a lower overall discharge, with no sudden changes or nonlinear behavior over the plotted range. The graph (5) shows that the wall shear stress τ_w increases as the Hartmann number M increases from 0 to 6, and the rise is nonlinear with a progressively steeper slope. At M≈0 the wall shear stress is about 1.5 Pa, then it grows

IARJSET ISSN (O) 2393-8021, ISSN (P) 2394-1588

International Advanced Research Journal in Science, Engineering and Technology

Impact Factor 8.311 ⁜ Peer-reviewed & Refereed journal ⁜ Vol. 13, Issue 1, January 2026

DOI: 10.17148/IARJSET.2026.13170

slowly for small M, but after about M≈2–3 it increases more rapidly, reaching roughly 4.2 Pa by M≈6. This trend indicates that stronger magnetic effects intensify the velocity gradient near the wall (even while the overall flow may be damped), leading to larger frictional stress at the boundary due to the formation of thinner, more strongly sheared near-wall regions. The graph (6) presents how wall shear stress τ_w varies along the axial position z across a stenosed (narrowed) region for three slip values β = 0.00, 0.20, and 0.40 mm. Far from the stenosis (|z| > 4 mm), τ_w is roughly constant and negative, with the most negative values occurring for β = 0 and becoming less negative as β increases. Entering the stenosed region (around z ≈ −4 mm), τw rises sharply, crosses from negative to positive, and forms a broad peak/plateau near the throat (approximately between z ≈ −2 and z ≈ 2 mm), indicating stronger near-wall velocity gradients where the vessel is constricted. As the flow exits the stenosis (near z ≈ 4 mm), τw drops rapidly back to the negative baseline level. Across the entire domain, increasing β shifts the curves upward, meaning higher slip parameter produces higher wall shear stress values (higher positive peak in the stenosis and less negative stress outside it).

VIII. CONCLUDING REMARKS

The analysis demonstrates that magnetic field intensity, wall slip, and yield stress strongly influence the flow dynamics of Casson blood in stenosed arteries. An increase in the Hartmann number enhances Lorentz forces, reducing the volumetric flow rate while steepening the velocity gradient near the wall, which increases wall shear stress. In contrast, introducing a finite slip at the arterial wall diminishes frictional resistance and moderates the shear stress distribution. The interplay between these parameters governs the overall hemodynamic behavior within the constricted region. The results highlight that magnetic fields can be effectively used to modulate blood flow, but excessive field strength may elevate wall stresses beyond physiological limits. Therefore, optimal control of magnetic and slip parameters can contribute to better biomedical applications such as targeted drug delivery, flow regulation, and diagnostic modeling in magnetically influenced vascular systems.

REFERENCES

[1]. Abrar M.N. (2025): "Entropy analysis of double diffusion in a Darcy medium with tangent hyperbolic fluid and slip factors over a stretching sheet: role of viscous dissipation," Numerical Heat Transfer, Part A: Applications, 86(10):3337–3350.

[2]. Imoro I., Etwire C.J., Musah R. (2024): "MHD flow of blood-based hybrid nanofluid through a stenosed artery with thermal radiation effect," Case Studies in Thermal Engineering, 59:104418.

[3]. Khan A.S., Abrar M.N., Uddin S., Awais M., Usman I. (2025): "Entropy generation due to micro-rotating Casson's nanofluid flow over a nonlinear stretching plate: numerical treatment," Waves in Random and Complex Media, 35(3):5243–5258.

[4]. Mirza A., Abdulhameed M., Shafie S. (2017): "Magnetohydrodynamic approach of non-Newtonian blood flow with magnetic particles in stenosed artery," Applied Mathematics and Mechanics (English Edition), 38(3):379–392.

[5]. Ponalagusamy R., Priyadharshini S. (2017): "Nonlinear model on pulsatile flow of blood through a porous bifurcated arterial stenosis in the presence of magnetic field and periodic body acceleration," Computer Methods and Programs in Biomedicine, 142:31–41.

[6]. Ramasekhar G., Shaik J., Reddisekhar Reddy S.R., Divya A., Jawad M., Yousif B.A.A. (2024): "Numerical investigation of Casson fluid flow performance of blood containing gold and Fe_3O_4 nanofluid injected into a stenotic artery," Numerical Heat Transfer, Part A: Applications, 1–17.

[7]. Reddy V.R.M., Reddy M.G., Mariserla B.M.K., Sandeep N. (2023): "Biosynthesis and numerical investigation of radiative heat transfer in silver-blood nanofluid flow through cosine-shaped stenosed artery: a biomedical application," Waves in Random and Complex Media, 1–17.

[8]. Sankar D.S., Lee U. (2011): "FDM analysis for MHD flow of a non-Newtonian fluid for blood flow in stenosed arteries," Journal of Mechanical Science and Technology, 25(10):2573–2581.

[9]. Sharma B.K., Gandhi R., Abbas T., Bhatti M.M. (2023): "Magnetohydrodynamics hemodynamics hybrid nanofluid flow through inclined stenotic artery," Applied Mathematics and Mechanics (English Edition), 44(3):459–476.

[10]. Sharma M.K., Bansal K., Bansal S. (2012): "Pulsatile unsteady flow of blood through porous medium in a stenotic artery under the influence of transverse magnetic field," Korea-Australia Rheology Journal, 24(3):181–189.

[11]. Sinha A., Shit G.C. (2015): "Modeling of blood flow in a constricted porous vessel under magnetic environment: An analytical approach", International Journal of Applied and Computational Mathematics ,1:219–234.

[12]. Tripathi J., Vasu B., Bég O.A., Gorla R.S.R. (2021): "Unsteady hybrid nanoparticle-mediated magneto-hemodynamics and heat transfer through an overlapped stenotic artery: biomedical drug delivery simulation,"

DOI: 10.17148/IARJSET.2026.13170

Proceedings of the Institution of Mechanical Engineers, Part H: Journal of Engineering in Medicine, 235(10):1175–1196.

[13]. Tripathi J., Vasu B., Gorla R.S.R., Chamkha A.J., Murthy P.V.S.N., Bég O.A. (2021): "Blood flow mediated hybrid nanoparticles in human arterial system: recent research, development and applications," Journal of Nanofluids, 10(1):1–30.

[14]. Turabi Y.U.U.B., Munir S., Nawaz R. (2024): "Entropy generation and magnetohydrodynamic influences on hybrid nanofluid convection in a staggered cavity," International Journal of Thermofluids, 27:101204.

[15]. Xenos M.A., Tzirtzilakis E.E. (2013): "MHD effects on blood flow in a stenosis," Advances in Dynamical Systems and Applications, 8(2):427–437.

